Steps and dislocations in cubic lyotropic crystals

2006 J. Phys.: Condens. Matter 18 6453

(http://iopscience.iop.org/0953-8984/18/28/002)

INSTITUTE OF PHYSICS PUBLISHING JOURNAL OF PHYSICS: CONDENSED MATTER

J. Phys.: Condens. Matter **18** (2006) 6453–6468 doi:10.1088/0953-8984/18/28/002

Steps and dislocations in cubic lyotropic crystals

S Leroy and P Pieranski

Laboratoire de Physique des Solides, Université Paris-Sud, Bâtiment 510, 91405 Orsay, France

Received 23 February 2006, in final form 25 May 2006
Published 28 June 2006
Online at stacks.iop.org/JPhysCM/18/6453

Abstract

It has been shown recently that lyotropic systems are convenient for studies of faceting, growth or anisotropic surface melting of crystals. All these phenomena imply the active contribution of surface steps and bulk dislocations. We show here that steps can be observed *in situ* and in real time by means of a new method combining hygroscopy with phase contrast. First results raise interesting issues about the consequences of bicontinuous topology on the structure and dynamical behaviour of steps and dislocations.

1. Introduction

1.1. Faceting and steps on surfaces of solid crystals

At the beginning of 19th century, René-Just Haüy hazarded a conjecture that faceted shapes of *solid crystals* reveal a three-dimensional periodic *positional* order of hypothetical molecules [1]. His visionary representations of crystal surfaces gave rise to the so-called Facet–Step–Kink (FSK) model [2, 3] that has been used, among others, by Burton *et al* [4]. Since their seminal paper on the theory of crystal shapes and growth, a considerable number of experimental studies proved that steps, forming closed loops or connected to bulk dislocations, really exist on surfaces of solid crystals grown from vapour or liquid phases (melt or solution) and that the order and motions of these steps determine the shapes of crystals. In particular, such steps have been detected by optical phase contrast microscopy [5], laser confocal microscopy [6], low-energy electron microscopy [7], scanning tunnelling microscopy [8] or by atomic force microscopy (AFM) [9]. Recently, the optical and AFM techniques have been combined in a study of spiraling steps on surfaces of KAP crystals growing from an aqueous solution [10].

1.2. Faceting and new surface phenomena in liquid crystals

The generic idea of the present work is that the three-dimensional periodic positional order of molecules, characteristic of a solid crystal, is not a necessary condition for faceting because certain *liquid crystals* can have faceted shapes as well. Among thermotropic mesophases, cholesteric blue phases [11, 12], smectic A [15, 16] and cubic phases [13, 14] can be quoted

as typical examples. Let us emphasize that in this last case, AFM microscopy has been used successfully for the detection of steps on free surfaces of supercooled samples.

In lyotropic systems, to our knowledge, the first observations of a faceting were made by Winsor [17] at a cubic/micellar interface and later by Sotta [18] on air bubbles included in the $Ia3d$ phase. Subsequently, faceting in lyotropic systems was studied in more detail by isoplethal and hygroscopic methods, and several new striking phenomena have been found to occur at cubic/isotropic interfaces [19].

- The *devil's staircase-type rich faceting* has been observed at $Ia3d$/vapour interfaces [20, 21]. As pointed out by Nozières, Pistolesi and Balibar (NPB) [22], the stability of vicinal facets with large Miller indices, seen as ordered systems of steps in terms of the FSK model, is due to a conjunction of a typical liquid/vapour interfacial tension with a very large size of unit cells.
- Lyotropic cubic phases can also form interfaces with three liquid isotropic phases: two micellar phases L1 and L2 and the sponge phase L3. In particular, experiments with the $Pn3m$/L1 interface [23, 24] have shown that its faceting is *poor*, in agreement with the NPB theory, because the tension of this interface between two liquid phases is much lower that of the former liquid/vapour one.
- In cases where cubic crystals are surrounded either by water vapour or by almost pure water, their shapes evolve under changes in humidity and/or temperature in spite of a constant surfactant content. The so-called *growth-by-redistribution* or the inverse *dismantling-by-redistribution* phenomena implied in these processes are specific for cubic liquid crystals formed with huge unit cells containing a variable number of molecules arranged into a partially liquid pattern. In terms of the FSK model, in the absence of bulk dislocations, these growth- and dismantling-by-redistribution phenomena should imply respectively nucleation or collapse of surface steps and their mobility. By analogy with solid crystals, these growth and dismantling mechanisms should be modified drastically in the presence of steps attached to dislocations, i.e. *Frank–Read sources*, in imperfect crystals [2–4, 26].
- Under a saw-tooth shaped temperature or humidity cycling, the so-called *ratchet-like effect* has been observed both at cubic/vapour and cubic/liquid interfaces [25]. In terms of the FSK model, this effect should be due to an asymmetry in the behaviour of steps during the alternating growth and dismantling episodes: during the growth, facets cannot progress because they are blocked by a prohibitive barrier for step nucleation, while during dismantling, facets recede because steps can always collapse.
- Shapes of cubic/vapour and cubic/liquid interfaces have been found to be very sensitive to temperature and/or humidity gradients [19]. As cubic liquid crystals are nothing else but organized solutions, this phenomenon can be seen as a manifestation of the *Ludwig–Soret effect* [19, 27, 28]. On a microscopic scale, these changes in shapes should also involve motions of steps.
- Finally, shapes and behaviour of steps should also be affected by the *facet-by-facet surface melting* phenomenon observed in the vicinity of cubic/L1 or cubic/L2 transitions [29, 30].

In the light of this enumeration, the observation of steps at lyotropic interfaces, *in situ* and in real time, appears as a means of a better microscopic description and understanding of these new faceting phenomena. Unfortunately, the quite rudimentary optical systems used so far in hygroscopic and isoplethal studies did not allow steps to be detected. Moreover, from experiments on facet-by-facet melting of $Ia3d$ monoolein/water crystals [19, 30] we learned that performances of the hygroscopic setup in terms of humidity and temperature control should be improved.

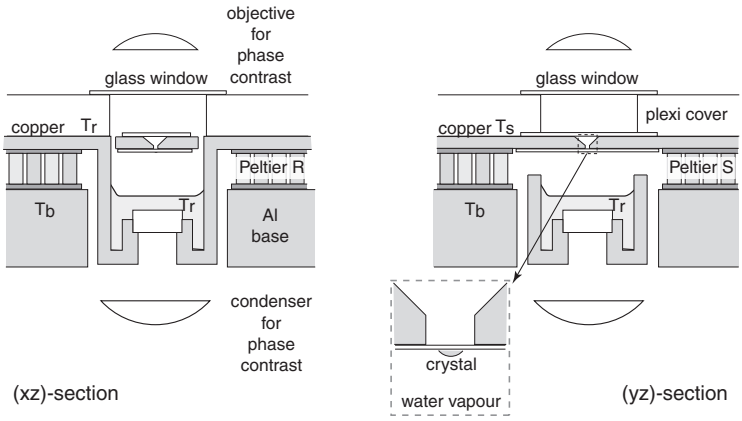

Figure 1. New setup for hygroscopic studies equipped with phase contrast. The temperatures T_r of the water reservoir and T_s of the sample holder are regulated independently, with respect to a thermalized aluminium base, by Peltier elements.

In this context, the conception of an new, improved hygroscopic setup dedicated to the observation of steps by phase contrast appeared as an experimental challenge.

The construction of this new setup is described in detail in the next section. Its performances have been checked for the first time on $Ia3d$ monoolein/water crystals. Results reported in sections 3 and 4 prove that our expectations have been satisfied: we were able to detect steps forming closed loops as well as steps connected to bulk dislocations on (112) and (220) facets of $Ia3d$ crystals. In the next section we prove, using general symmetry arguments, that the observed features of steps connected to dislocations agree with the theoretical relationship involving orientations of Burgers vectors, belonging to the body-centred cubic (bcc) Bravais lattice, with respect to facets. The discussion of this relationship is continued in the penultimate section in terms of the nodal approximation of the $Ia3d$ bicontinuous structure [31]. In particular, topological constraints imposed on surfaces and bulk dislocations by bicontinuous structures of cubic phases are considered.

2. Hygroscopic setup dedicated to observation of steps

2.1. Humidity control

The setup depicted schematically in figure 1 can be qualified as a hygroscope of third generation. In the first system used for studies of the devil's staircase faceting of $Ia3d$/vapour interface [20], humidity control was achieved by mixing dry and 100% humid gas fluxes. Experiments with $C_{12}EO_6$, monoolein, DTACl and DDMAS have shown however that cubic phases occur generally in the humidity range between 95 and 100% where this system of humidity control is not the most accurate. For this reason, the principle of humidity control was changed in the next version of the hygroscope [30]: the sample was enclosed in an almost tight metallic cell containing a small reservoir of water and the relative humidity at the sample level was a function of the temperature difference between water, in good thermal contact with the cell, and the sample whose temperature was regulated independently. In order to improve the accuracy of this system, the third generation system shown in figure 1 consists of three parts.

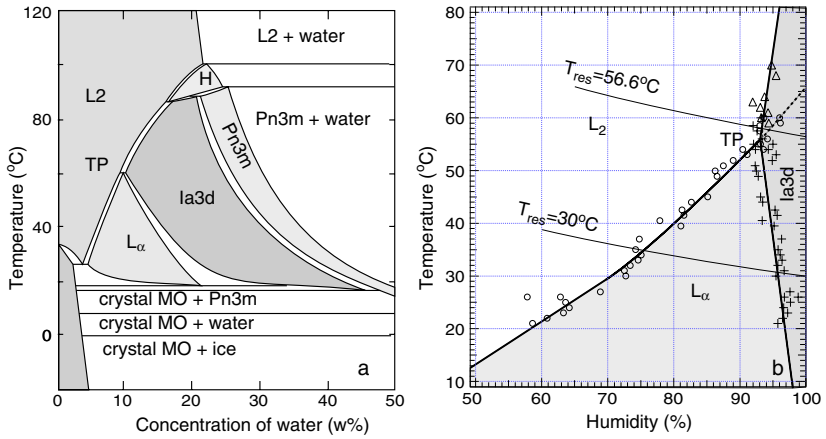

Figure 2. Phase diagrams of monoolein. (a) Temperature versus concentration from [32]. (b) Temperature versus humidity from [30]. Nucleation of $Ia3d$ monocrystals from L2 droplets occurs when the L2 $\rightarrow$ $Ia3d$ transition is crossed along an isothermal path a few degrees above the triple point TP. Dashed lines correspond to trajectories followed when the temperature T_r of the water reservoir is kept fixed and the temperature of the sample is varied.

(This figure is in colour only in the electronic version)

(i) Large aluminium base of thickness 1.5 cm. Its temperature T_b is regulated by circulation from a water bath.
(ii) Reservoir of water, made of copper. The (xz)-section shows that it is supported by two Peltier elements that regulate its temperature T_r.
(iii) Sample holder, made of copper. The (yz)-section shows that it is supported by a second pair of Peltier elements that regulate its temperature T_s.

In practice, the temperatures T_r and T_s are regulated with accuracy better than 0.01 °C. As explained in [30], the relative humidity H at the sample level is given by the formula

$$H(T_s, T_r) = \frac{p_s(T_r)}{p_s(T_s)} \times 100\% \tag{1}$$

where $p_s(T)$ expresses the dependence of the saturated vapour pressure at temperature T. Knowing the accuracy $\delta T = \pm 0.01$ °C of temperature regulations, the corresponding accuracy of the humidity control is about $\delta H = \pm 0.05\%$. Let us note that the sample holder has a smaller thermal inertia than the water reservoir. For this reason, in order to change the humidity, it is more convenient to keep the temperature T_r of the water reservoir constant and to vary the temperature $T_s = T_r + \Delta T$ of the sample holder. As a consequence, the T versus H phase diagram is explored along slightly oblique paths, such as those indicated by dashed lines in figure 2. For each path two parameters are pertinent: $\mathbf{T}_r = \mathbf{const}$ and $\mathbf{\Delta T} = \mathbf{T}_s - \mathbf{T}_r$.

2.2. Optical phase contrast

The second major improvement in the new hygroscopic setup consists in using the phase contrast optical set: a matched condenser–objective pair from a biological microscope. As the light beam from the condenser passes through the layer of water, the capillarity-induced curvature of the water surface can perturb the condenser–objective matching. For this reason, the diameter of the water reservoir was made large enough (≈3 cm) to keep the water surface flat. Images have been taken with a CCD camera.

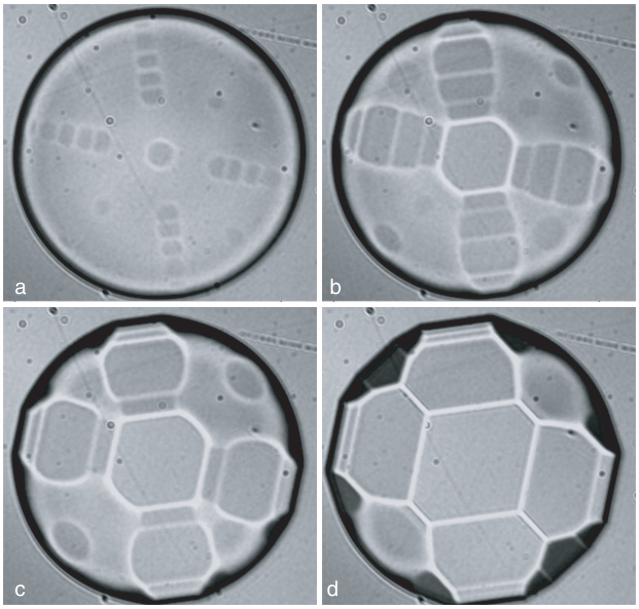

Figure 3. Enlargement of the (220) facet on an $Ia3d$ crystal of monoolein by the ratchet effect. Shapes (a)–(d) were obtained by four consecutive saw-tooth shaped humidity cycles. Let us emphasize that in these photographs, obtained in transmitted light without phase contrast, steps are not visible.

2.3. Know-how of genesis and shaping of $Ia3d$ crystals

First experiments have shown that steps at the $Ia3d$/vapour interface are easily visible in phase contrast only when they are located on large principal facets (112) or (220) orthogonal to the optical axis. To satisfy these requirements, the following procedure was used.

(i) *Materials*: Experiments were made with $Ia3d$ crystals of monoolein/water system studied previously by hygroscopy [19, 30]. The main reason for this choice is that it offers favourable conditions for the generation of $Ia3d$ monocrystals.

(ii) *Genesis of $Ia3d$ crystals*: From the temperature versus humidity phase diagram of monoolein in figure 2 it results that at temperatures above 65 °C nucleation of $Ia3d$ monocrystals from L2 droplets occurs when the L2 $\rightarrow$ $Ia3d$ transition line is crossed along an isothermal path T_r = const passing above the triple point TP.

(iii) *Orientation of $Ia3d$ crystals*: $Ia3d$ crystals have to be oriented with (112) or (220) principal facets parallel to the mica substrate. As explained in [30], orientations of $Ia3d$ crystals obtained by the L2 $\rightarrow$ $Ia3d$ transition are usually random. Therefore, the sequence of transitions L2 $\rightarrow$ $Ia3d$ $\rightarrow$ L2... was repeated until the suitable (112) and (220) orientations were obtained.

(iv) *Ratchet-like growth of facets*: Once a monocrystal with a suitable orientation has been nucleated from a L2 droplet, saw-tooth shaped cycles of humidity, contained in the humidity range of the $Ia3d$ phase, were applied. The purpose of this operation is enlargement of principal facets by the ratchet-like effect discussed in [25] and illustrated here by the series of four photographs in figure 3.

Let us emphasize that large facets generated by this procedure seem to be perfectly smooth when observed in transmitted light without phase contrast.

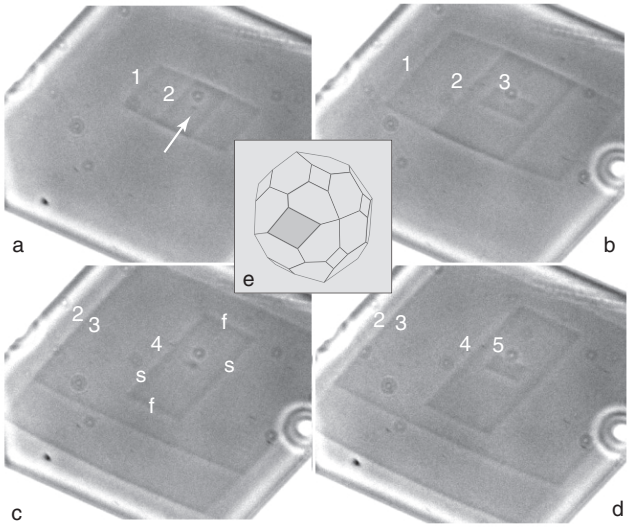

Figure 4. Nucleation and growth of elementary steps on the (220) facet of an $Ia3d$ crystal subsequent to a steep decrement of humidity $\Delta H = -0.5\%$. ((a)–(d)) Pictures taken at intervals of 3 s. Numbers label steps in the order of their nucleation from the dust particle indicated in (a) by the arrow. The mobility of steps is anisotropic. Edges s and f of the step 4 in (c) are respectively slow and fast. This anisotropy is identical in step 2 but inverted in steps 1, 3 and 5. The height of steps is $d_{220} = 35$ Å. (e) $Ia3d$ crystal habit composed of (112) and (220) sets of facets.

3. Steps forming closed loops

3.1. Nucleation and growth of steps on (220) and (112) facets

As the first example of the efficiency of the new hygroscopic setup equipped with phase contrast we show in figures 4 and 5 nucleation and growth of steps on (220) and (112) facets of a $Ia3d$ crystal similar to the one in figure 3. Prior to the nucleation of steps, the two control parameters $T_r = 60\,^\circ$C and $\Delta T = T_s - T_r = 0.6\,^\circ$C were kept fixed for several minutes. The purpose of this preliminary annealing is to 'clean' the facet, that is to say, to let the preexisting steps reach the borders of facets or collapse.

After annealing, the nucleation of new steps is triggered by a steep increment $\Delta T = 0.1\,^\circ$C of the sample temperature corresponding, following equation (1), to a decrement $\Delta H = -0.5\%$ of humidity.

From previous experiments with monoolein we know that the unit cells of $Ia3d$ crystals shrink when the humidity decreases and as a consequence new cells must be created. If the humidity variation rate $\mathrm{d}H/\mathrm{d}t$ were to slow, the growth-by-redistribution mechanism would lead to the formation of new unit cells exclusively on rough parts of the crystal surface. In the hygroscopic setup, the order of magnitude of this rate is given by $\Delta H/\tau_{th}$, where τ_{th}, the characteristic time of the temperature regulation, is of the order of 15 s. Typically, when $\Delta T > 0.02\,^\circ$C (i.e. $\Delta H < -0.1\%$), heterogeneous nucleation of steps on facets occurs.

In figure 4, steps are labelled by numbers $1 \ldots 5$ indicating the order of their nucleation from the dust particle pointed out by the arrow. These first five steps, nucleated in a short time interval of 3 s after the decrement of humidity, are followed by other steps. The total number of nucleated steps depends on the amplitude of the decrement ΔH as well as on the thickness of the crystal. Typically, for $\Delta H = -0.5\%$, about 20 steps are nucleated. It is clear from

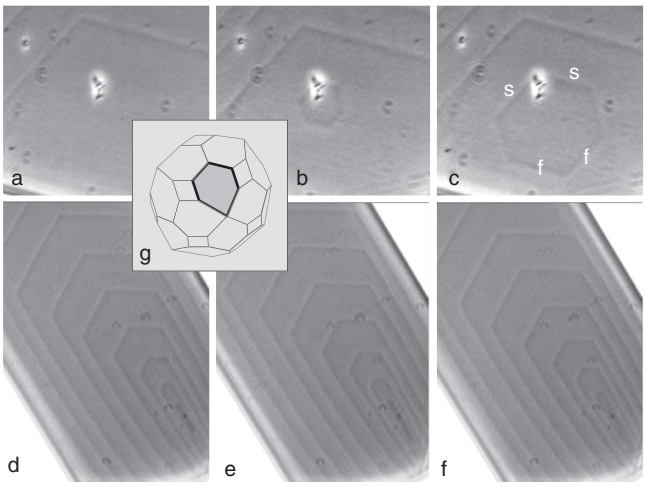

Figure 5. Nucleation and growth of elementary steps on a (112) facet of an $Ia3d$ crystal of monoolein. ((a)–(c)) Nucleation of a step on a dust particle. The mobility of steps is anisotropic. Edges s and f are respectively slow and fast. ((d)–(f)) System of growing steps. All steps are identical. (g) $Ia3d$ crystal habit composed of (112) and (220) sets of facets.

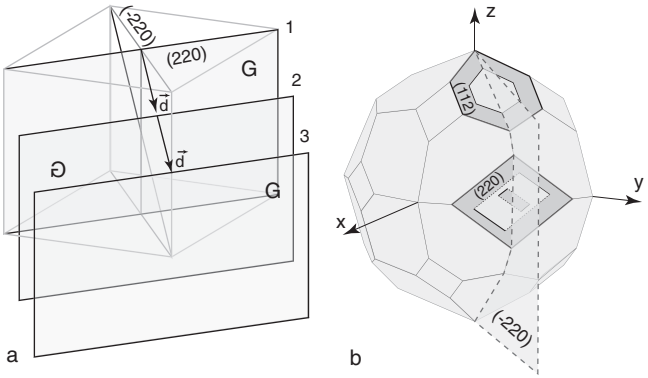

Figure 6. Role of the glide plane d on the shapes of steps. (a) Definition of the glide plane. (b) Symmetry of steps induced by the glide plane d.

the series of four pictures in figure 4 that the mobility of steps on this facet is anisotropic. For example, edges s and f of step 4 in picture (c) are respectively slow and fast. This anisotropy is identical for step 2 and for all even steps but is inverted for steps 1, 3, 5 and, in general, for all odd steps.

Figure 5 illustrates nucleation and growth of steps on the (112) facet. The first three pictures ((a)–(c)) show nucleation of a new step on a dust particle and its subsequent anisotropic growth. Obviously, the mobility of this step is also anisotropic: edges s are slow while f are fast. The three other pictures ((d)–(f)) prove that, unlike on the (220) facet, all steps nucleated on the (112) facet have identical anisotropic mobilities.

3.2. Shapes of steps and $Ia3d$ symmetry

This striking difference in shapes of steps on (220) and (112) facets, summarized in figure 6(b), reveals in fact the $Ia3d$ symmetry of the lyotropic crystal. Indeed, one of special features of

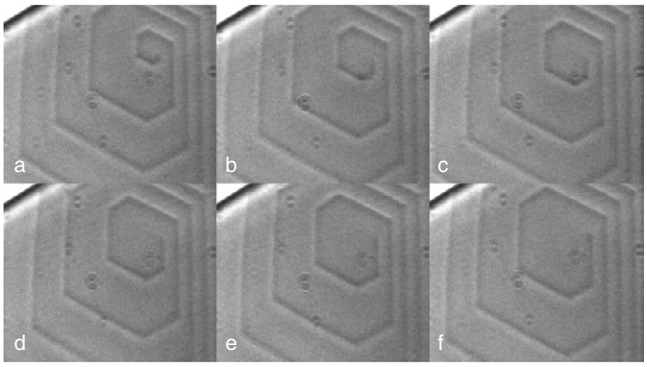

Figure 7. Spiral shaped step connected to a dislocation emerging on a (112) facet.

this space group is that it contains non-symmorphic symmetry operations such as the glide plane d. As shown in figure 6(a), this symmetry operation consists in a mirror reflection in the $(\bar{2}20)$ plane followed by the partial translation $\vec{d}$ (along the diagonal axis $[11\bar{1}]$) of length d_{222}.

Now, as shown in figure 6(b), both (220) and (112) facets are orthogonal to the mirror plane $(\bar{2}20)$. However, the partial translation $\vec{d}$ has different orientations with respect to these facets. On the one hand, $\vec{d}$ is parallel to the (112) facet and much shorter than it. Therefore, the shape of an elementary step of height d_{211} on this facet is invariant with respect to the mirror reflection. Let us emphasize that if the height of the step were a multiple of d_{211}, the same would be true. On the other hand, $\vec{d}$ is oblique with respect to the (220) facet so that the mirror reflection links now two successive elementary steps of height d_{220}, in agreement with experiments.

We can conclude therefore on a symmetry basis that the steps shown in figure 4 are elementary. For the steps shown in figure 5, we can only conjecture that they are elementary because in practice their optical contrast is the lowest one. The heights of the steps can be deduced from x-ray studies of the monoolein/water system [32]. Knowing the size of the cubic unit cell, $a \approx 100$ Å, one gets respectively $h = d_{220} \approx 35$ Å and $h = d_{112} \approx 41$ Å.

4. Steps connected to dislocations

After successful visualization of steps forming closed loops, our next challenge was to find steps 'with ends', connected to dislocations emerging on facets. We have found that on very clean facets (without nucleation centres), a large decrement in humidity $\Delta H \approx -1.5\%$ corresponding to $\Delta T \approx +0.3\,^{\circ}\mathrm{C}$ results in the generation of spiral shaped steps. Why and how dislocations connected to such steps are created is a question that we will not try to answer here.

4.1. Dislocations emerging on (112) facets

In figure 7 we show a typical spiral shaped step connected to a dislocation emerging on a (112) facet. In the real-time video sequence taken during a growth-by-redistribution episode, the observer has an impression of seeing a rotating spiral. In fact, this series of pictures taken at intervals of $1/10$ s shows that motions of the step and of the dislocation are more complex.

Another example of steps connected to dislocations is shown in figure 8. In this texture, two different types of dislocation, 1 and 2, are emerging on the (112) facet. Dislocation 1

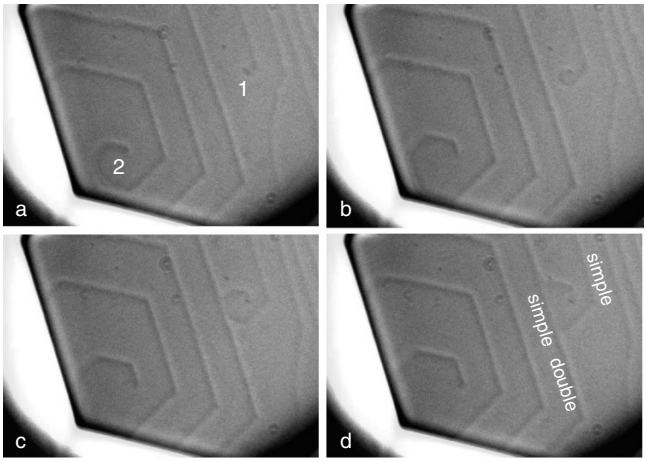

Figure 8. Steps of two different heights, simple and double, connected to dislocations, 1 and 2, emerging on a (112) facet. During the growth-by-redistribution process, steps are moving and the double step splits into two simple steps.

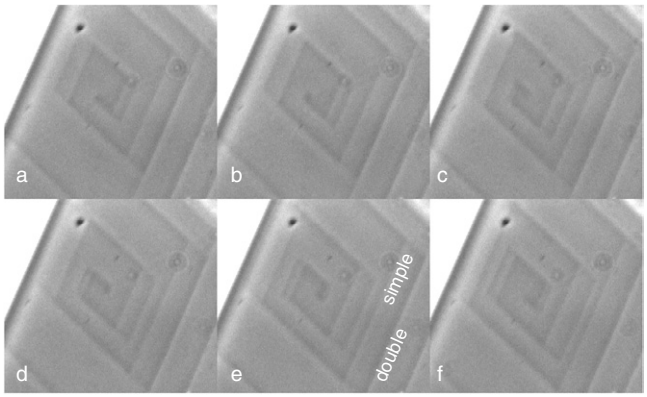

Figure 9. Pair of spiral shaped steps connected to the dislocation emerging on the (220) facet. Series of pictures taken at intervals of 0.3 s during a growth-by-redistribution episode.

is connected to an optically thin step while dislocation 2 is connected to a thick step. This sequence of four images taken at intervals of 1/4 s shows that the thick step labelled 'double' splits into two thin steps labelled 'simple'.

In all other observations only these two types of dislocation have been identified.

4.2. Dislocations emerging on (220) facets

On the (220) facet, dislocations of only one type always with two elementary steps connected to them were observed. An example of the double spiral formed by these two steps during the growth-by-redistribution process is shown in figure 9. It has a peculiar shape due to the anisotropic mobilities of the two steps discussed previously in section 3.1.

To understand this feature of growth spirals on the (220) facet better, let us consider the schemes in figure 10(a) representing the configuration of two elementary spiral shaped

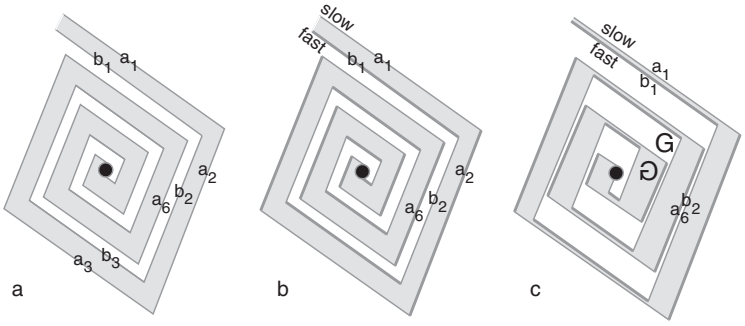

Figure 10. Pair of spiral shaped steps connected to the dislocation emerging on the (220) facet. (a) Decomposition of steps into segments a_i and b_i. (b) Fast and slow segments drawn respectively with thick and thin lines. (c) Fast segments catch up slow ones.

steps connected to the dislocation. These steps, a and b, are composed of segments: a_1, a_2, a_3 ... for one step and b_1, b_2, b_3 ... for the second one. We know from section 3.1 that differently oriented pairs of segments on closed-loop steps have different mobilities, slow and fast, alternating from step to step. For this reason, segments drawn with thick and thin lines in figure 10(b) are respectively fast and slow. During the growth, the first segment b_1 of the step b is fast so it catches up the slow one a_1 of the step a and subsequently the two steps form a pair a_1b_1 moving together (figure 10(c)). The next segment b_2 of the step b is slow so it is caught up by the fast segment a_6 of the step a. Subsequently, the pair b_2a_6 is moving together. As a result, segments of the two steps are generally associated into pairs $a_{2n+1}b_{2n+1}$ alternating with pairs $b_{2n}a_{2n+4}$. When the direction of steps changes, pairs $a_{2n+1}b_{2n+1}$ are dissociated into simple steps that recompose again into pairs $b_{2n}a_{2n+4}$.

5. Relationship between steps and dislocations

5.1. General rules

In order to deepen the interpretation of results concerning steps connected to dislocations we have first to recall the dislocation–step relationship involved in the Frank–Read growth mechanism [22, 26, 3].

Let $\vec{b}$ be the Burgers vector of the dislocation drawn in figure 11 and $\vec{t}$ its director (a unit vector parallel to the dislocation line). In the simplest text-book configuration shown in figure 11(a), a pure screw dislocation with $\vec{b} \parallel \vec{t}$ is orthogonal to the facet. At its point of emergence on the facet, there starts a step of height $h = |\vec{b}|$. In contrast, the facet stays flat when the dislocation emerging at the facet is of the pure wedge type with $\vec{b} \perp \vec{t}$ (figure 11(b)).

In the most general case (figures 11(c) and (d)), the formation of the step connected to the emerging dislocation is determined by the Burgers vector $\vec{b}$ alone; the direction of the dislocation $\vec{t}$ does not matter. More precisely, the height h of step is equal to the component $b_\perp$ of the Burgers vector perpendicular to the facet. We have therefore to examine orientations of Burgers vectors with respect to (220) and (112) facets.

For energetic reasons, only the shortest Burgers vectors have to be considered. In the case of $Ia3d$ crystals having the bcc Bravais lattice, the shortest Burgers vectors connect the centre of the cubic unit cell with its vertices (figure 12).

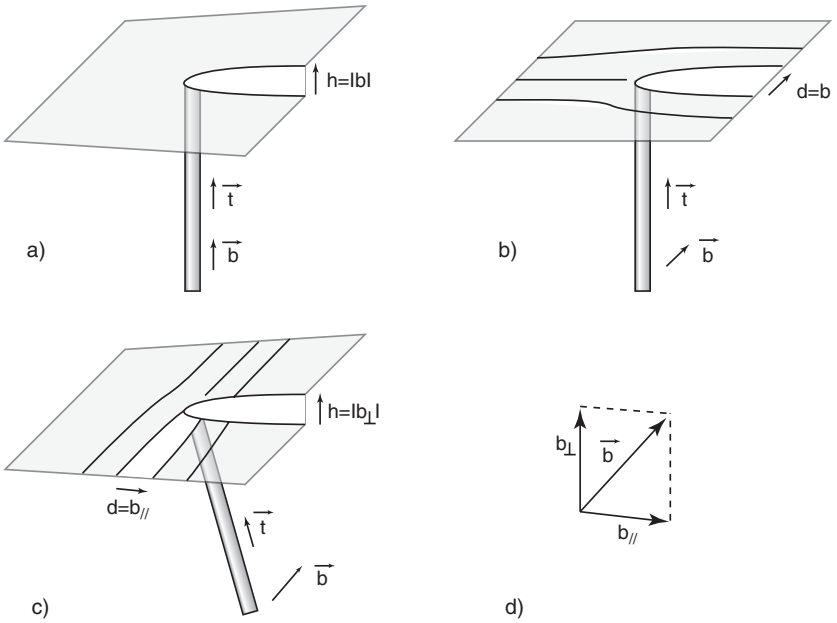

Figure 11. Relationship between dislocations emerging on a facet and corresponding steps.

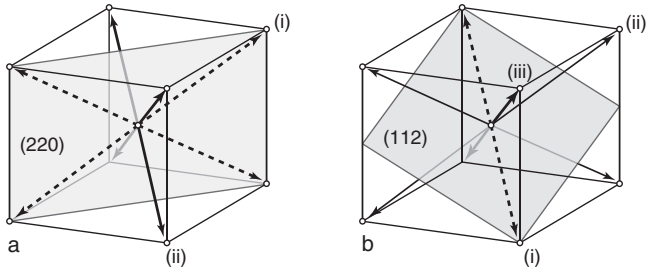

Figure 12. Orientations of Burgers vectors with respect to facets. (a) (220) facet: two types, (i) and (ii), of Burgers vector. (b) (112) facet: three types, (i), (ii) and (iii), of Burgers vector.

5.2. Step–dislocation relationship, (220) facets

In the case of the (220) facet (figure 12(a)), this set of eight Burgers vectors splits into two subsets:

(i) the four vectors drawn with dashed lines are parallel to the facet and do not produce steps,
(ii) the four other vectors drawn with plain lines form the same angle with the facet and have the same orthogonal component $b_\perp = 2d_{220}$.

In conclusion, dislocations emerging on the (220) facet either do not produce any step or produce double steps.

5.3. Step–dislocation relationship, (112) facets

In the case of the (112) facet (figure 12(b)), the set of eight Burgers vectors splits into three subsets:

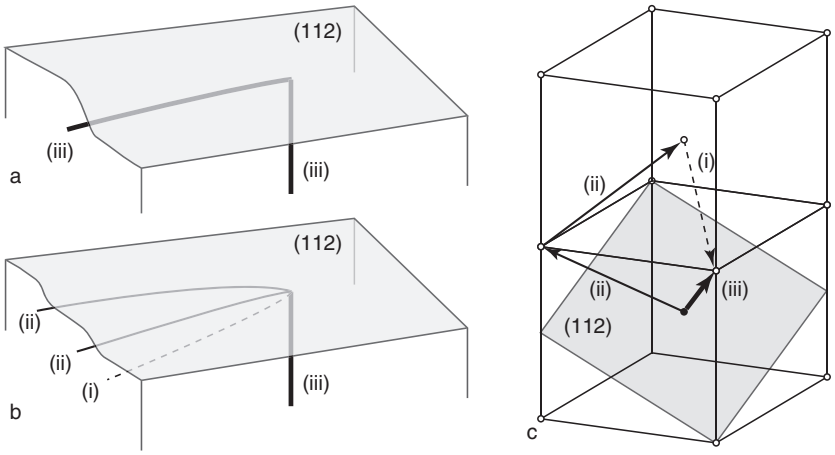

Figure 13. Splitting of steps due to dissociation of buried dislocations. (a) Buried dislocation of type (iii) producing a double step on the (112) facet. Its Burgers vector is drawn with a thick plain line in (c). (b) Dissociation of the dislocation of type (iii) into two dislocations of type (ii) producing simple steps and one dislocation of type (i). (c) Conservation law of Burgers vectors of dissociated dislocations.

(i) the two vectors drawn with dashed lines, parallel to the facet, do not produce steps,
(ii) the four vectors drawn with thin plain lines form the same (small) angle with the facet and have the same orthogonal component $b_\perp = d_{112}$,
(iii) the two vectors drawn with thick plain lines form the same (large) angle with the facet and have the same orthogonal component $b_\perp = 2d_{112}$.

In conclusion, dislocations emerging on the (112) facet can produce either simple or double steps.

6. Structures of facets and steps

All the above considerations about steps and dislocation were made exclusively on the basis of the $Ia3d$ symmetry. It is however tempting to take into account special features of the $Ia3d$ cubic lyotropic phase such as its elastic softness and its bicontinuous structure.

6.1. Steps or buried dislocations in soft crystals?

In terms of the faceting theory of *soft crystals* developed by Nozières *et al* [22], steps occurring on surfaces of soft crystals could in fact be due to dislocations buried below the crystal/vapour interface. Are our observations compatible with this model? This question should in particular be addressed to the case of double steps attached to dislocations of type (iii) emerging on (112) facets. Experiments reported in section 4 tell us that one double step on a (112) facet can split into two simple steps (see figure 8). Let the double step be due to a buried dislocation of type (iii) (see figure 13(a)) with Burgers vector [111]/2 drawn with a thick plain line in figure 13(c). Then, the two simple steps could be due to buried dislocations of type (ii) (see figure 13(b)) with Burgers vectors $[1\bar{1}1]/2$ and $[\bar{1}11]/2$. However, such a splitting of one dislocation of type (iii) into two dislocation of type (ii) would not satisfy the conservation law of Burgers vectors. In fact, in addition to these two dislocations of type (ii), one dislocation of type (i) with the

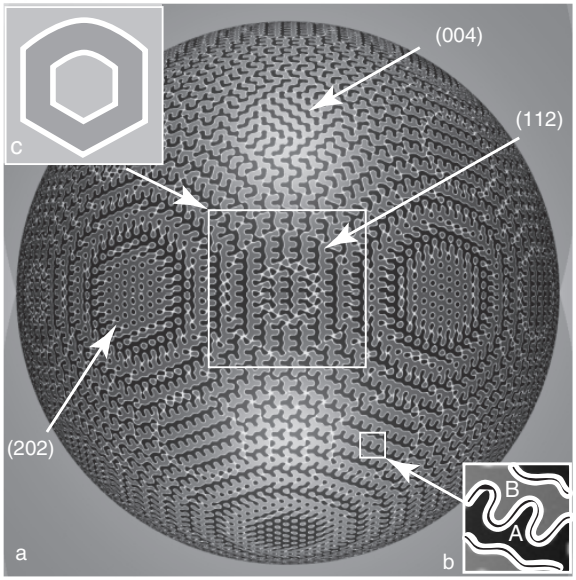

Figure 14. Spherical cross-section of the bicontinuous $Ia3d$ structure. The lower inset shows water labyrinths A and B separated by bilayer. The upper inset shows two steps formed on the (112) facet.

Burgers vector $[11\bar{1}]/2$ also results from this splitting in agreement with:

$$\left[\tfrac{1}{2}, \tfrac{1}{2}, \tfrac{1}{2}\right] = \left[-\tfrac{1}{2}, \tfrac{1}{2}, \tfrac{1}{2}\right] + \left[\tfrac{1}{2}, -\tfrac{1}{2}, \tfrac{1}{2}\right] + \left[\tfrac{1}{2}, \tfrac{1}{2}, -\tfrac{1}{2}\right]. \tag{2}$$

As this third dislocation is of type (i), with its Burgers vector parallel to the (112) facet, it does not give rise to a step and cannot be detected by optical phase contrast.

In conclusion, if the steps observed in our experiments were due to buried dislocations, the observed splitting of double steps into simple steps would correspond to splitting of one emerging dislocation into three buried dislocations. Such a process that seems to have an unfavourable energetic balance has not been considered in [22].

6.2. Reconstruction of the $Ia3d$/vapour interface

In the opposite limit of steps located at the crystal/vapour interface, the bicontinuous topology of the $Ia3d$ phase may play an important role. Indeed, the $Ia3d$ cubic phase of monooelein has an inverted bicontinuous structure in which the surfactant bilayer has shape of the gyroid IPMS separating two labyrinths related by the inversion symmetry and filled with water. In the bulk of a perfect crystal, the surfactant bilayer is supposed to be continuous, without edges, but on the surfaces, some reconstruction must occur. To imagine what kind of reconstruction is plausible, let us examine the spherical cross-section of a perfect $Ia3d$ crystal shown in figure 14(a). This drawing was made by means of the Pov-Ray freeware using the *isosurface* command with the function

$$f(x, y, z) = \cos(x) * \sin(y) + \cos(y) * \sin(z) + \cos(z) * \sin(x) \tag{3}$$

invariant with respect to the $Ia3d$ space group. In figure 14(a), water labyrinths A and B, represented respectively in grey and black, are separated by the surfactant bilayer drawn as a double white line in figure 14(b). The edges of the bilayer cut by the sphere can be healed at least by two processes.

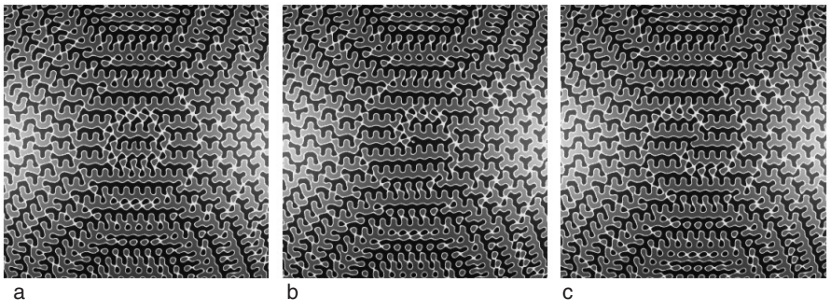

Figure 15. Emergence of dislocations on the (112) facet: (a) type (i) (b) type (ii), (c) type (iii) (types defined in figure 12(b)).

(i) One can use patches of appropriate shapes made of a bilayer and 'sew' them on one of the labyrinths. As a result, this labyrinth is enclosed inside the bilayer while the second one remains open. This process, which breaks the A–B symmetry [24, 31], would be appropriate if the bicontinuous phase were surrounded by water.
(ii) One can also use patches made of a monolayer and 'sew' them on the two labyrinths. This process seems to be more appropriate in the case of $Ia3d$/vapour interface because it introduces surfactant monolayers at water/vapour interfaces, like in soap bubbles. It preserves the A–B inversion symmetry of the $Ia3d$ phase.

6.3. Steps on reconstructed $Ia3d$/vapour interface

Let us suppose that the reconstruction of the second type occurs effectively at the $Ia3d$/vapour interface so that the bright lines in the spherical cross-section in figure 14(a) can be seen as linear defects due to splitting of the bilayer into the two monolayers. In order to minimize the energy of these defects, regions with low and high density of these defects will form respectively extended terraces and localized steps [33].

Following this ad hoc model, reconstruction of the pattern in the centre of the cross-section in figure 14(a) leads to the formation of the two steps on the (112) facet depicted in figure 14(c).

6.4. Steps and dislocations

Using the same software, we have also drawn spherical cross-sections of $Ia3d$ crystals with dislocations emerging on facets. In figures 15 and 16 we show patterns due to all types of dislocation defined previously (see figure 12). In agreement with experiments,

on the (112) facet:

(i) a dislocation of type (i) with its Burgers vector parallel to the facet does not produce steps,
(ii) a dislocation of type (ii) with its Burgers vector oblique to the facet produces one elementary steps,
(iii) a dislocation of type (iii) with its Burgers vector almost normal to the facet produces two elementary steps;

on the (220) facet:

(i) a dislocation of type (i) with its Burgers vector parallel to the facet does not produce steps,
(ii) a dislocation of type (ii) with its Burgers vector oblique to the facet produces two elementary steps.

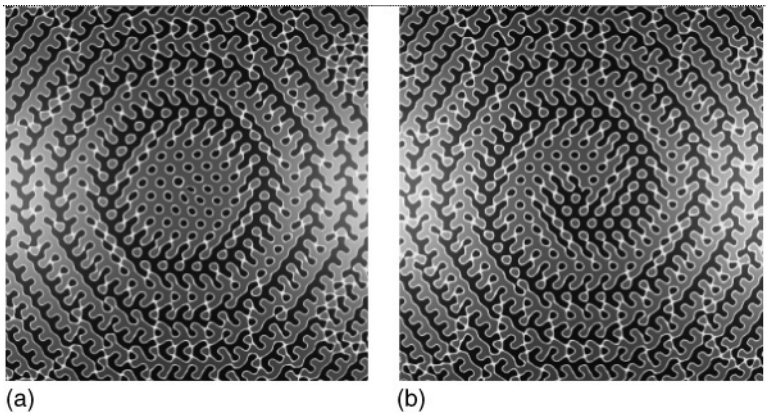

Figure 16. Emergence of dislocations on the (220) facet: (a) type (i) (b) type (ii) (types defined in figure 12(a)).

7. Conclusions and perspectives

The new hygroscopic setup equipped with optical phase contrast fulfilled our expectations. Using it, several new significant results have been obtained.

- Steps on (112) and (220) facets have been detected.
- We have shown that steps can either form closed loops or be attached to dislocations emerging on facets.
- By means of appropriate humidity variations, we were able to control the nucleation, collapse and changes in size and shape of closed-loop steps as well as the nucleation and evolution of steps connected to dislocations.
- Polygonal shapes taken by steps during growth episodes revealed that the mobilities of steps are anisotropic. In particular, the alternating anisotropy of successive steps on the (220) facet is a fingerprint of the glide plane d typical of the $Ia3d$ symmetry.
- The occurrence of simple and double steps connected to dislocations emerging on the (112) facet is also a fingerprint of the bcc Bravais lattice of the $Ia3d$ symmetry group.

Let us note these all results reported here, obtained for the first time with $Ia3d$ crystals of monooelein, have been confirmed in all details in subsequent experiments with $Ia3d$ crystals of phytantriol (which has a T versus H phase diagram [30] similar to the one of monoolein).

In the near future, we intend to apply the new hygroscopic setup for more detailed studies of phenomena enumerated in the introduction. In particular, the facet-by-facet surface melting [30] deserves more attention. Indeed, preliminary experiments have shown that shapes of steps depend much on the 'distance' ΔH from the $Ia3d \rightarrow$ L2 transition line. Roughly speaking, for large ΔH, the growth shapes of steps are polygonal, made of straight segments meeting at sharp angles, while in the vicinity of the $Ia3d \rightarrow$ L2 transition, these angular discontinuities disappear and steps become rough. One can therefore speculate that melting of facets and changes in shapes of steps are related.

Acknowledgments

We thank V Klein, S Saranga, J-L Signoret and J-P Dallac for technical assistance. We are also very grateful to Madame Sylvie Messager from Laserson Chimie Fine for providing us with a sample of phytantriol.

References

[1] Haüy R-J 1801 *Traité de minéralogie*
[2] Nozières P 1992 Shape and growth of crystals *Solids Far From Equilibrium* ed C Godrèche (Cambridge: Cambridge University Press)
[3] Villain J and Pimpinelli A 1995 *Physique de la Croissance Cristalline* (Paris: Eyroles)
[4] Burton W K, Cabrera N and Frank F C 1951 *Trans. R. Soc. London* A **243** 299
[5] Tsukamoto K 1983 *J. Cryst. Growth* **61** 199
[6] Sazaki G, Matsui T, Tsukamoto K, Usami N, Ujihara T, Fujiwara K and Nakajima K 2004 *J. Cryst. Growth* **262** 536
[7] Kodambaka S, Khare S V, Swieciech W, Ohomori K, Petrov I and Green J E 2004 *Nature* **429** 49
[8] Ranganathan M, Dougherty D B, Cullen W G, Zhao T, Weeks J D and Williams E D 2005 *Phys. Rev. Lett.* **95** 225505
[9] Bonzel H P 2003 *Phys. Rep.* **385** 1
[10] McLoughlin M J, Mays T J and Price R 2005 *Phys. Rev. Lett.* **95** 115504
[11] Blümel T and Stegemeyer H 1984 *J. Cryst. Growth* **66** 163
[12] Barbet-Massin R, Cladis P E and Pieranski P 1984 *Phys. Rev.* A **30** 1161
[13] Even C, Gourbil A, Impéror-Clerc M, Pieranski P and Veber M 2002 *J. Chem. Phys.* **12** 1031
[14] Even C, Imperor-Clerc M and Pieranski P 2006 *Eur. Phys. J.* E **20** 89
[15] Bechhoefer J and Oswald P 1991 *Eur. Phys. Lett.* **15** 521
[16] Bechhoefer J, Lejcek L and Oswald P 1992 *J. Physique* II **2** 27
[17] Winsor P A 1974 *Liquid Crystals and Plastic Crystals* vol 2 (Amsterdam: Ellis Horwood) (chapter 5, figure 5.13)
[18] Sotta P 1991 *J. Physique* II **1** 763
[19] For a review see Pieranski P 2005 *J. Phys.: Condens. Matter* **17** S3333
[20] Pieranski P, Sotta P, Rohe D and Imperor-Clerc M 2000 *Phys. Rev. Lett.* **84** 2409
[21] Pieranski P, Sittler L, Sotta P and Imperor-Clerc M 2001 *Eur. Phys. J.* E **5** 317
[22] Nozières P, Pistolesi F and Balibar S 2001 *Eur. Phys. J.* B **24** 387
[23] Lynch M L, Kochvar K A, Burns J L and Laughlin R G 2000 *Langmuir* **16** 3537
[24] Pieranski P, Bouchih M, Ginestet N and Popa-Nita S 2003 *Eur. Phys. J.* E **12** 239
[25] Plötzing T and Pieranski P 2004 *Eur. Phys. J.* E **13** 179
[26] Friedel J 1964 *Dislocations* (Oxford: Pergamon)
[27] Piazza R and Guarino A 2002 *Phys. Rev. Lett.* **88** 208302
[28] Wiegand S 2004 *J. Phys.: Condens. Matter* **16** R357
[29] Grenier J, Plötzing T, Rohe D and Pieranski P 2006 *Eur. Phys. J.* E **19** 223
[30] Leroy S, Grenier J, Rohe D, Even C and Pieranski P 2006 *Eur. Phys. J.* E **20** 19
[31] See for example Schwarz U S and Gompper G 1999 *Phys. Rev.* E **59** 5528
[32] Qiu H and Caffrey M 2000 *Biomaterials* **21** 223
[33] Fournier J-B 2005 private communication